Reversibility of the synthesis-decomposition reaction in the ball-milled Cu-Fe-O system

1998 J. Phys.: Condens. Matter 10 11829

(http://iopscience.iop.org/0953-8984/10/50/020)

J. Phys.: Condens. Matter **10** (1998) 11829–11840. Printed in the UK PII: S0953-8984(98)96365-2

Reversibility of the synthesis–decomposition reaction in the ball-milled Cu–Fe–O system

G F Goya† and H R Rechenberg

Instituto de Física, Universidade de São Paulo, CP 66318, 05315-970/SP São Paulo, Brazil

Received 30 July 1998, in final form 7 October 1998

Abstract. In this work, we present results from a ball-milling experiment carried out simultaneously on (a) $CuFe_2O_4$ spinel and (b) its precursor mixture $CuO + \alpha$-Fe_2O_3, to investigate their evolution under identical conditions. Partial reversibility of the reaction $CuO + \alpha$-$Fe_2O_3 \leftrightarrow CuFe_2O_4$ was observed, resulting in nearly equal phase composition for both systems after 420 h of milling. X-ray data showed that the final admixture was composed mainly of nanosized α-Fe_2O_3 and spinel phases. Almost coincident average grain sizes $\langle d \rangle \approx 14$ nm were found in both milled samples, although different size distributions were inferred from their magnetic behaviour. Superparamagnetic (SPM) relaxation effects were observed in the resulting particles at room temperature. Mössbauer and magnetization data taken below the SPM blocking temperature indicate partial formation of the $Cu_xFe_{3-x}O_4$ ($0 < x < 1$) spinel solid solution, with cubic structure and high local disorder.

1. Introduction

Structural and magnetic properties of nanosized particles can be strikingly different from those of the same bulk materials [1–3]. The magnetic phenomena associated with nanosized systems include macroscopic magnetic tunnelling, superparamagnetism (SPM) and spin canting [4–8], making these novel systems of interest in material science and engineering [9]. Mechanical grinding and alloying are becoming a standard procedure to obtain nanosized materials and metastable phases [10, 11]. Although theoretical and empirical models of microstructural evolution, collision frequency and impact energy during the milling process have been proposed [12], the fundamental mechanisms involved are not yet fully understood. Ball milling is usually considered as a means of obtaining solid-state reactions, which occur across the welded interfaces of the powder particles when impacted by the grinding media. All solid-state reactions involve the formation of product phases that displace the reactants. As this process is governed by the geometry and diffusion rates of the reactants and products, it requires relatively high temperatures (i.e. several hundred degrees) to overcome the energy barrier. Mechanical milling minimizes the energy barrier of the products by increasing the reaction interface, through continuously welding and fracturing the powder particles at the nanometre scale. This allows chemical reactions to take place at nearly room temperature. Mössbauer spectroscopy provides a helpful tool to study the evolution of milled phases, by measuring the local hyperfine interactions of the probe atom, which can sense minute changes in the local crystalline structure and magnetic properties of the system. We present in this work x-ray, Mössbauer and magnetization results on samples of $CuFe_2O_4$ and its

† Corresponding author. E-mail address: goya@macbeth.if.usp.br.

0953-8984/98/5011829+12$19.50

precursor mixture CuO+α-Fe_2O_3, ball-milled under identical conditions. The main purpose was to perform a comparative study regarding the microstructural and magnetic properties of the resulting Cu–Fe–O phases after milling.

2. Experimental procedure

Polycrystalline $CuFe_2O_4$ spinel was prepared by mixing stoichiometric amounts of α-Fe_2O_3 and CuO powders (99.999% purity, $\approx$200 μm particle size) and heating in air at 1200 K for 20 hours, repeating the procedure three times. The final cooling ramp was set to 2 K min^{-1} to avoid the formation of cubic phase. This was one of the starting samples used in the milling experiment, which will be labelled CFS hereafter. The second sample used in the experiment was a 1:1 mixture of CuO and α-Fe_2O_3, thought of as a precursor for the formation of $CuFe_2O_4$. This sample will be labelled CFM. Each sample was placed in a separate container and milled in a planetary ball mill (Fritsch Pulverisette 7), with hardened steel ($Fe_{74}Cr_{18}Ni_8$) vials and balls, for 420 h. Rotational velocity was 950 rpm, and a ball-to-powder mass ratio of 12:1 was chosen. Equal weights of starting powders were used in each container of the planetary miller, whereby the single process ensured identical milling conditions for both samples. Acetone was added to the containers as a carrier liquid, to give high particle mobility during milling. The resulting powders were dried in air at 323 K. X-ray diffraction data of these samples did not show detectable signs of contamination from the vials and balls. X-ray diffraction measurements were performed using a Philips PW-1140 diffractometer with Cu Kα radiation in the 2θ range of 10–80° with a step size of 0.01°. Mössbauer measurements were performed with a conventional constant-acceleration spectrometer in transmission geometry with a ^{57}Co source in a Rh matrix at 4.2 and 296 K. All isomer shifts are given relative to that of α-Fe at room temperature. Optimal absorber thickness was calculated to be 18 mg cm^{-2}. Mössbauer spectra were fitted using Lorentzian lineshapes, and a shape-independent distribution fitting program [13] was used when hyperfine field distributions were present. Magnetization measurements were performed in a vibrating sample magnetometer at 4.2 K and 300 K, in fields up to 90 kOe.

3. Experimental results

Figures 1(a) and (b) show the x-ray data corresponding to as-prepared $CuFe_2O_4$ and CuO+α-Fe_2O_3 samples (CFS and CFM respectively). The starting CFM mixture shows the expected peaks corresponding to CuO and α-Fe_2O_3 phases. The initial $CuFe_2O_4$ sample was found to be single phase, with tetragonal structure and lattice parameters $a = 8.225(2)$ Å and $c = 8.691(2)$ Å. For milled CFM and CFS samples, figures 1(c) and (d) evidence a remarkable similitude of XRD patterns, having almost identical peak positions and intensities. In order to check the possibility of this similitude being originated in sample inhomogeneities, a second set of measurements was performed on different fractions of sample, with identical results. Average grain sizes $\langle d \rangle$ were estimated from XRD data using the Scherrer equation, after subtracting instrumental broadening from the experimental linewidth. The values obtained for milled CFM and CFS samples were $\langle d \rangle = 14(2)$ nm and $\langle d \rangle = 13(2)$ nm, respectively. The comparative analysis of the x-ray patterns of figure 1 showed that large amounts of α-Fe_2O_3 are present in both milled samples. A second phase with spinel structure was also observed. Since the potentially produced phases have similar Bragg reflections, a conclusive identification of this phase was unattainable due to the large broadening of the experimental x-ray lines. However, it can be noticed that the peak at

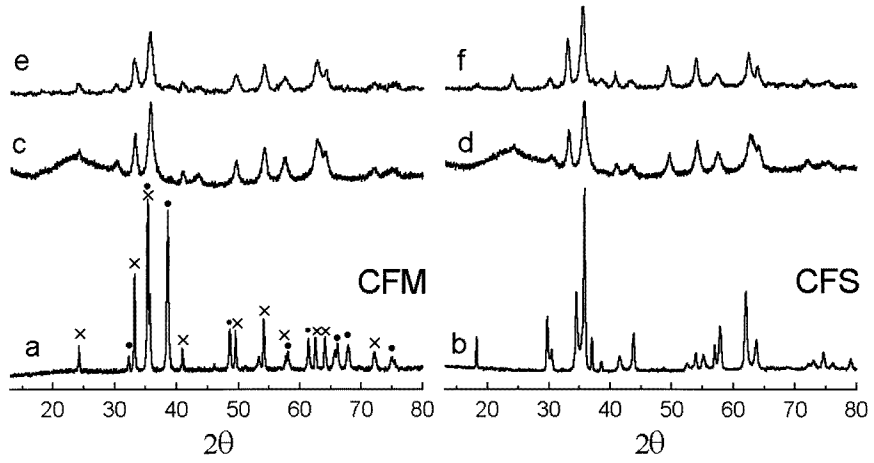

Figure 1. X-ray data of as-prepared (a) CFM and (b) CFS samples; (c) CFM and (d) CFS samples milled 420 h. Patterns for milled CFM and CFS samples with further annealing at 623 K are shown in (e) and (f), respectively. Peaks corresponding to the starting α-Fe_2O_3 ($\times$) and CuO ($\bullet$) phases are shown.

$2\theta = 34.5^\circ$ distinctive of tetragonal $CuFe_2O_4$ spinel is absent, suggesting a tetragonal-to-cubic transformation of the spinel phase during milling. These features suggest that the solid solution $Cu_xFe_{3-x}O_4$, with $0 < x < 1$, is formed during milling. Small amounts of CuO were also detected, with the strongest peaks near the limit of XRD detection. Table 1 shows the experimental peak position of milled samples, and those corresponding to the starting CuO, α-Fe_2O_3 and $CuFe_2O_4$ phases [14]. The background curvature observed at low angles is related to the carrier liquid used in the milling process, which remains strongly bounded to the grains. Accordingly, this feature disappears after heating the samples at 673 K for 1 h, as shown in figures 1(e) and 1(f). It can be observed that both patterns remain essentially unchanged after annealing, with the same peak positions and relative intensities as the as-milled patterns. The average grain sizes found were 34(5) nm and 31(5) nm, for annealed CFM and CFS samples respectively.

To further investigate the phase composition of milled samples, Mössbauer measurements were performed at 296 and 4.2 K. Room temperature Mössbauer spectra of as-prepared CFM and CFS samples are shown in figure 2. The spectrum of sample CFM consists simply of a sextet (with hyperfine field $B = 51.6$ T), corresponding to bulk α-Fe_2O_3 at room temperature [15]. For the starting CFS sample, two sextets were observed, with hyperfine parameters corresponding to Fe^{3+} at A and B sites of the spinel structure, coincident with previously reported data [16, 17]. These parameters are summarized in table 2. Mössbauer spectra at $T = 296$ K of CFM and CFS samples milled for 420 h are shown in figure 3. For the milled CFM sample, the spectrum was composed of one sextet and a central doublet (figure 3(a)). The isomer shift and quadrupole splitting values of the central doublet are in agreement with previously reported data for superparamagnetic α-Fe_2O_3 particles [15]. The observed magnetic signal has hyperfine parameters corresponding to bulk α-Fe_2O_3, showing that a fraction of the initial large particles (above the SPM critical size) is still present after milling. For the milled CFS sample the central doublet in the spectrum has, within errors, the same parameters as those in the CFM sample (see table 2). To stress this similitude between the two central doublets, the inset of figure 3

Table 1. Relative intensities (I) of Bragg reflections at position 2θ of samples CFM and CFS milled for 420 h. Peak positions of α-Fe_2O_3, CuO, tetragonal (t) and cubic (c) $CuFe_2O_4$ phases are given for comparison.

CFM		CFS		α-Fe_2O_3		CuO		t-$CuFe_2O_4$		c-$CuFe_2O_4$	
2θ (°)	I (%)	2θ (°)	I (%)	2θ (°)	I (%)	2θ (°)	I (%)	2θ (°)	I (%)	2θ (°)	I (%)
24.3	38	24.3	41	24.2	30	32.4	8	18.2	17	18.5	30
30.3	27	30.3	28	33.2	100	35.4	100	29.8	32	30.2	50
33.3	61	33.2	61	35.7	70	38.6	92	30.5	13	35.6	100
35.7	100	35.8	100	41.0	20	48.7	21	34.5	53	37.2	10
40.9	15	41.0	16	49.5	40	58.1	11	35.9	100	43.0	30
43.5	14	43.5	15	54.1	45	61.4	16	37.0	14	57.1	40
49.6	28	49.6	33	57.7	10	66.3	13	41.5	11	62.8	60
54.3	43	54.1	48	62.5	30	68.1	13	43.8	22	74.5	20
57.7	32	57.5	31	64.2	30	75.1	7	53.9	10	79.5	10
62.7	53	63.0	54	72.0	10			55.5	12		
64.1	36	64.3	36	75.4	8			57.9	24		
71.9	15	72.1	17					62.1	40		
75.3	13	75.3	14					63.7	16		

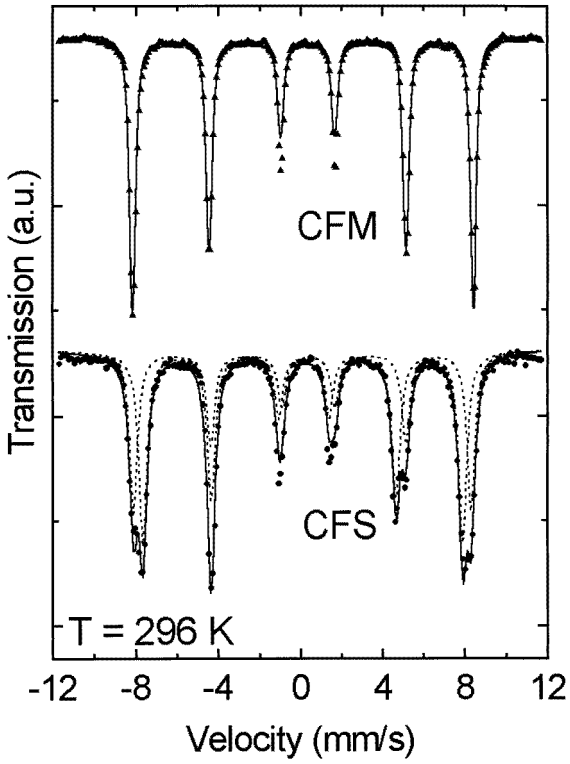

Figure 2. Room temperature Mössbauer data of starting CFM and CFS samples. Solid lines are the total fitted spectra, whereas dotted lines correspond to each component.

shows the resulting curve after subtracting the CFS from the CFM spectrum, where only the magnetic part is left. A single broad line was added to fit both spectra at 296 K, to account

Table 2. Mössbauer parameters of as-prepared and milled CFM and CFS samples, at $T = 296$ K: hyperfine field (B), isomer shift (δ), quadrupole splitting (Δ), linewidth (Γ) and relative spectral area (I).

			B (T)	δ (mm s^{-1})	Δ (mm s^{-1})	Γ (mm s^{-1})	I (%)
As-prepared	CFM	H1	51.6(1)	0.36(1)	−0.23(2)	0.27(1)	100(2)
	CFS	H1	51.1(1)	0.35(1)	−0.11(2)	0.38(1)	45(3)
		H2	48.2(1)	0.28(1)	0.00(2)	0.44(1)	55(3)
Milled 420 h	CFM	H1	51.1(1)	0.37(1)	−0.22(2)	0.38(1)	23(4)
		D1	—	0.35(1)	0.58(2)	0.33(2)	17(2)
		L1	—	0.33(2)	—	1.8(1)	60(6)
	CFS	D1	—	0.33(1)	0.60(2)	0.45(2)	29(4)
		L1	—	0.47(2)	—	1.6(1)	71(8)

Table 3. Mössbauer parameters of samples CFM and CFS milled for 420 h, taken at $T = 4.2$ K: hyperfine field (B), isomer shift (δ), quadrupole splitting (Δ), linewidth (Γ) and relative spectral area (I) for each site. Errors are quoted between parentheses.

Sample	Parameters	H1	H2	H3	H4
CFM	B (T)	54.3(2)	53.2(2)	52.1(2)	—
	δ (mm s^{-1})	0.50(1)	0.49(1)	0.42(1)	—
	Δ (mm s^{-1})	0.06(2)	−0.10(2)	−0.18(2)	—
	Γ (mm s^{-1})	0.31(3)	0.37(3)	0.52(4)	—
	I (%)	17(3)	52(4)	31(4)	—
CFS	B (T)	—	52.9(2)	51.3(2)	49.8(2)
	δ (mm s^{-1})	—	0.49(1)	0.46(1)	0.52(1)
	Δ (mm s^{-1})	—	−0.20(1)	−0.09(1)	0.07(2)
	Γ (mm s^{-1})	—	0.33(2)	0.46(3)	0.76(4)
	I (%)	—	54(3)	33(4)	13(4)

for relaxation effects and particle size distributions. This signal corresponds to the fraction of particles near the SPM critical size, i.e. having relaxation times close to the Mössbauer measuring time τ_m [18].

In order to slow down superparamagnetic relaxation, Mössbauer measurements were performed at $T = 4.2$ K, well below the blocking temperature T_B. The two spectra (figure 4(a)) display differences regarding the opposite asymmetry of the outer lines (1 and 6) and the broader lines of CFM sample at positive velocities. These differences suggest the existence of non-resolved magnetic components or hyperfine field distributions. The resulting distribution profiles showed three distinct field contributions in both cases (figures 4(b) and 4(c)), which accounted for the major features of the spectra. Based on these results, we analysed the data more simply using only three sites for each spectrum. As shown in table 3, the hyperfine fields obtained in this way match the values of each maximum of the distribution profiles. The H1 signal with $B = 54.3(2)$ T in the FM sample is coincident with the value for bulk α-Fe_2O_3 at this temperature [15, 19], in agreement with the contribution from large particles observed in the room temperature spectrum. Based on previous measurements on nanosized $CuFe_2O_4$ at $T = 4.2$ K [20], the H2 and H3 magnetic signals observed in the milled CFM sample were assigned to A and B sites in the spinel structure. For α-Fe_2O_3 particles with sizes below $d \approx 20$ nm, a reduction of the hyperfine field is expected, due to magnetic collective excitations [19]. As observed by

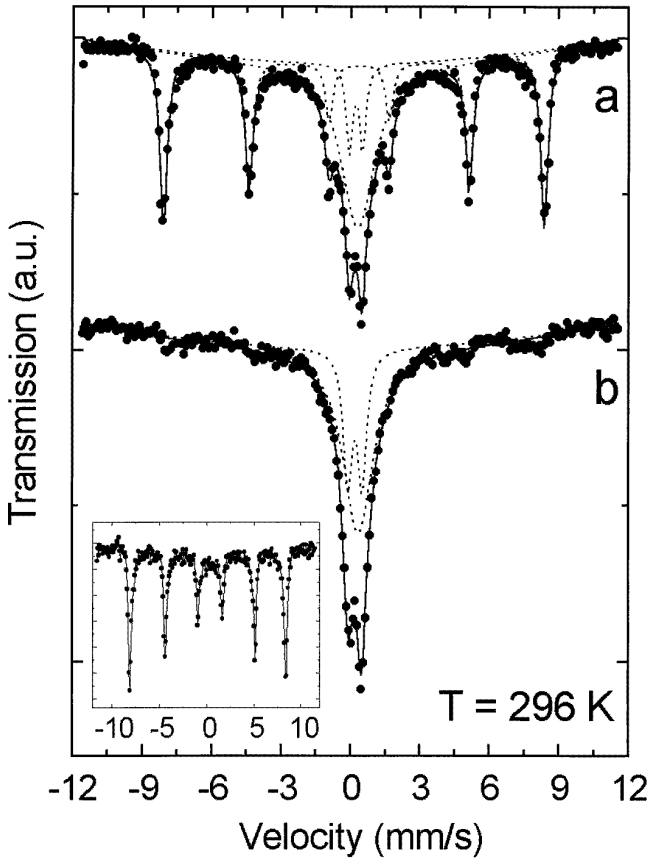

Figure 3. Room temperature Mössbauer data of (a) CFM and (b) CFS samples milled for 420 h. Solid lines are the fitted spectra, and dotted lines correspond to each component. The inset shows the difference between CFM and CFS spectra, where the solid line is drawn to emphasize the structure of the sextet.

Kündig *et al* [15], the hyperfine field in haematite nanoparticles (of diameter $d \approx 18$ nm) was reduced to about $B \approx 53$ T at low temperatures. The large spectral area observed for the H2 signal ($B = 53.2$ T) in the CFM sample could therefore be originated in two unresolved contributions from Fe^{3+} at (1) α-Fe_2O_3 particles with $d \leqslant 20$ nm, and (2) the B sites of the copper spinel. The Mössbauer spectrum of the milled CFS sample at 4.2 K showed no indication of an H1 signal, in agreement with the absence of large α-Fe_2O_3 particles observed at room temperature. The H2 signal in the CFS sample also shows a large resonant area as found in the CFM sample, suggesting similar unresolved contributions from small α-Fe_2O_3 particles and B sites in $CuFe_2O_4$. In addition to the H2 and H3 signals from $CuFe_2O_4$, a new sextet H4 with hyperfine field $B = 49.8(2)$ T and linewidth $\Gamma = 0.76(4)$ mm s^{-1} is observed. The small hyperfine field and broad lines are related to sample regions with oxygen vacancies and/or high local disorder produced during milling. We associate these features with the formation of sample regions with $Cu_xFe_{3-x}O_y$ stoichiometry (see discussion below) [21].

Mössbauer measurements of annealed samples did not show evidence of SPM relaxation

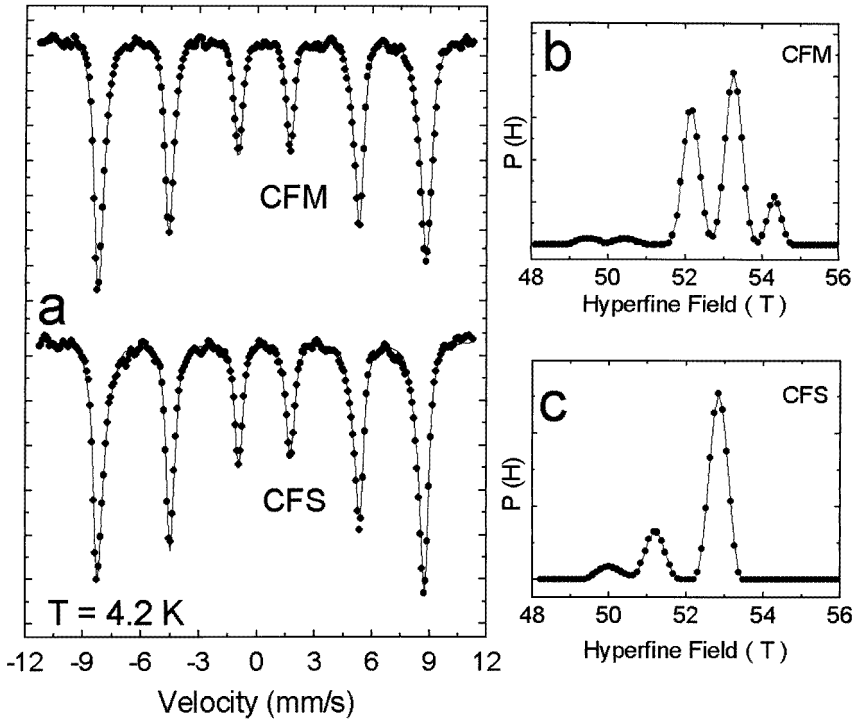

Figure 4. (a) Mössbauer spectra of milled CFM and CFS samples taken at $T = 4.2$ K. The fits to the experimental data are shown with solid lines. The resulting hyperfine field distributions for CFM and CFS samples are shown in (b) and (c), respectively.

at room temperature (figure 5), in agreement with the larger grain sizes deduced from XRD data. For both spectra, the asymmetry of the magnetic lines indicates unresolved low-field contributions, and thus hyperfine field distributions were used to fit the data. The similitude between the resulting distribution profiles of CFM and CFS samples is remarkable, with the main component centred at $B \approx 51$ T, and a minor distribution at lower fields ($B < 50$ T). In both cases, the maximum of the distribution is associated with the added contributions from α-Fe_2O_3 and spinel phases. The observed distributions at $B < 50$ T indicate that, even after annealing, a noticeable amount of local disorder of the Fe^{3+} environments is still present in both samples.

Figure 6 shows magnetization data for milled CFS and CFM samples, at $T = 300$ and 4.2 K. The saturation magnetization M_s, coercive force and remanence to saturation ratio values at both temperatures are given in table 4. The values of magnetization M_s at $H = 90$ kOe for milled CFS and CFM samples are comparable at room temperature. The value $M_s \approx 20$ emu g^{-1} is considerably smaller than the $M_s \approx 33$ emu g^{-1} of bulk $CuFe_2O_4$ spinel [22, 23]. On the other hand, this value is much higher than that predicted for the CFM sample assuming only contributions from the starting CuO and α-Fe_2O_3 oxides. It is also observed that full saturation is not reached at fields of $H = 90$ kOe, suggesting a spin canted structure formed during the milling process in both systems. At $T = 300$ K both milled samples are superparamagnetic for the measuring times ($\tau \approx 100$ s) involved in magnetization measurements, as seen from the nearly zero coercive fields H_c. The larger

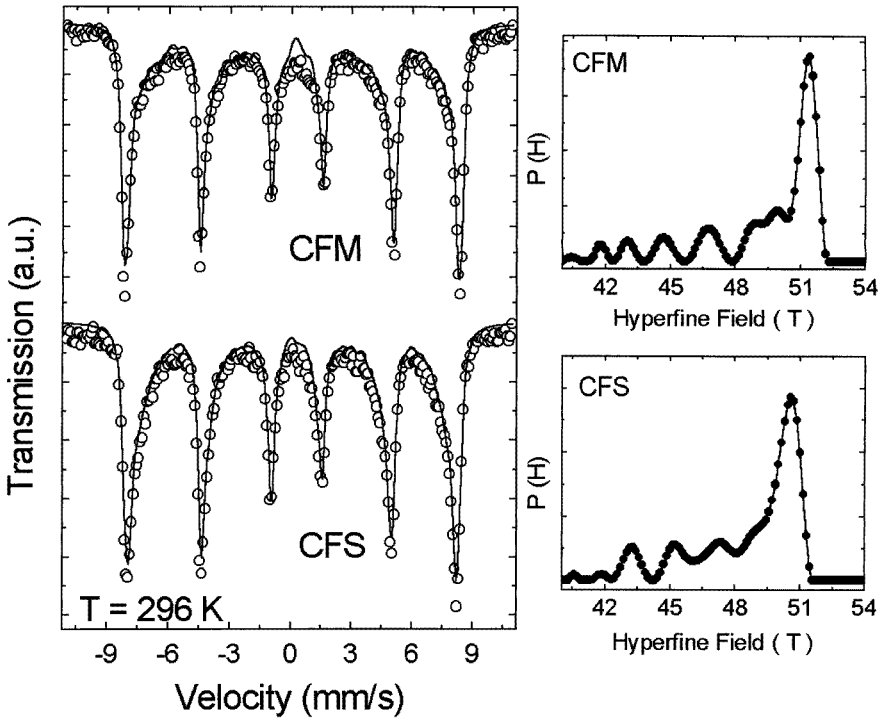

Figure 5. Room temperature Mössbauer spectra of milled CFM and CFS samples after annealing at 673 K by 1 h. The fitted spectra are shown with solid lines, together with the obtained hyperfine field distributions.

Table 4. Magnetization at $H = 90$ kOe (M_s), coercive field (H_c) and remanence/magnetization ratio (M_r/M_s) values, for milled CFM and CFS samples, measured at 4.2 and 300 K. Errors are quoted between parentheses.

		M_s (emu g^{-1})	H_c (kOe)	M_r/M_s
CFM	$T = 4.2$ K	19.2(1)	0.74(1)	0.44
	$T = 300$ K	19.4(1)	0.18(2)	0.15
CFS	$T = 4.2$ K	20.4(1)	0.69(1)	0.46
	$T = 300$ K	19.1(1)	0.18(2)	0.14

H_c values observed at $T = 4.2$ K originate from the blocking of the magnetic moments at this temperature. The values of M_r/M_s below T_B are close to the theoretical value of 0.5 for uniaxial, noninteracting single domain particles randomly oriented.

4. Discussion

Although XRD data of both as-prepared CFM and CFS samples show clearly distinguishable peaks, the corresponding patterns of milled samples show the evolution towards a similar phase composition. This fact indicates that chemical reactions take place during milling. The possibility of producing chemical transformations through mechanical energy has been

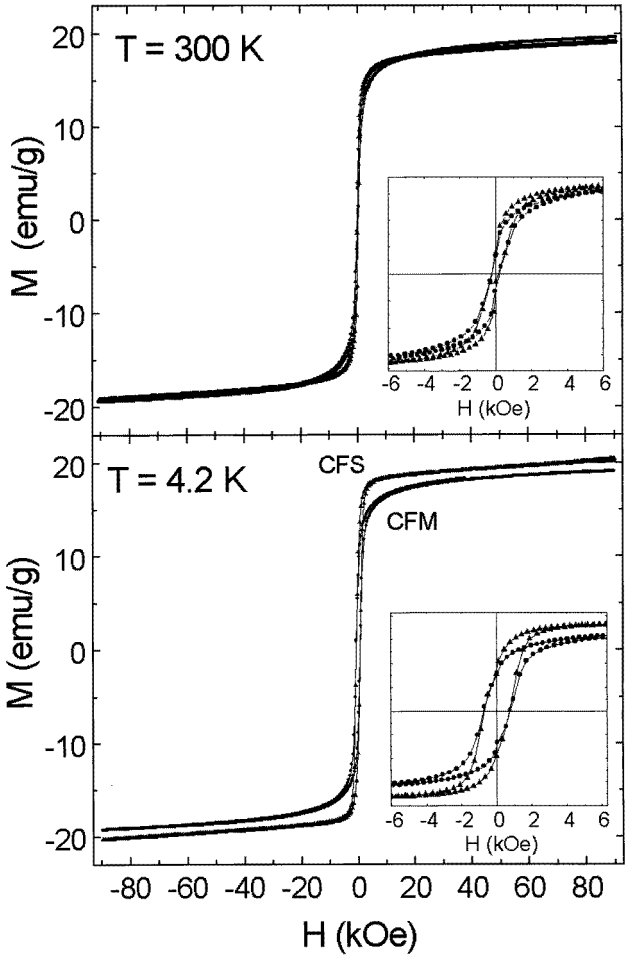

Figure 6. Magnetization curves, up to $H = 90$ kOe, taken at $T = 300$ K and $T = 4.2$ K for milled CFM and CFS samples. The insets show the low field regions.

extensively demonstrated in metallic as well as in oxide systems [1, 24–27]. Matteazzi and Le Caër [28] have shown that chemical reduction of haematite to nanocrystalline wüstite can be achieved by dry ball milling, using carbon as a reducing element. Similarly, recent experiments performed by Linderoth *et al* [29] have demonstrated the reversibility of the reaction α-$Fe_2O_3 \leftrightarrow Fe_3O_4$, depending on the milling conditions. The study of solid reactions induced by mechanical energy (mechanochemistry) and mechanosynthesis of metastable compounds has given rise to the concept of tribochemical equilibrium [30], which is strongly associated with the conditions under which the reaction takes place.

In previous work on milled $CuFe_2O_4$ samples [20], we found that chemical reactions which took place during milling resulted in α-Fe_2O_3 and CuO segregation, and subsequent formation of the $Cu_xFe_{3-x}O_4$ solid solution and magnetite. It was proposed that the chemical reaction $CuFe_2O_4 \rightarrow \alpha$-$Fe_2O_3 + Cu_xFe_{3-x}O_4 + y(CuO + Cu) + O_2$ could account for the observed transformations, in particular the molar ratio of $(CuO + Cu)$ to α-Fe_2O_3 phases. In the present milling experiment, the tiny amounts of CuO phase observed suggest that

similar mechanisms may be operative.

It is well known that, for ball-milled powders, the final phases can show a high degree of microstructural disorder. As the oxygen vacancies produced by milling break the Fe–O–Fe superexchange paths, the average magnetic field at an Fe site is expected to decrease. Within the spinel ferrite structure, the A–B interactions are stronger than the A–A or B–B interactions. Additionally, in $CuFe_2O_4$ the Fe^{3+}–O–Cu^{2+} superexchange interactions are weaker than the corresponding Fe^{3+}–O–Fe^{3+} [31, 32]. Therefore, the redistribution of Cu^{2+} and Fe^{3+} ions between A and B sites of the spinel structure can effectively modify the superexchange interactions, lowering the local field of a given Fe^{3+} site. The local disorder at Fe sites, originating in these mechanisms, lowers the observed hyperfine fields and produces a distribution of iron coordinations that broaden the resonant line. The magnetic component with the lowest hyperfine field and large linewidth observed in milled samples is likely to be due to this kind of locally disordered Fe site produced during milling.

Iron reduction from α-Fe_2O_3 to Fe_3O_4 has been detected in ball milling experiments using closed containers [20, 29]. In spite of the difficulty of indexing the characteristic XRD peaks due to line broadening, the presence of magnetite can be identified by the increase of the magnetic moment, since $M_s(Fe_3O_4) = 98$ emu g^{-1}. In our present experiment, the low saturation magnetization of milled samples, even lower than the $M \approx 34$ emu g^{-1} of the $CuFe_2O_4$ phase indicates that formation of Fe_3O_4 was not an important reaction during milling. The values of magnetization of milled samples can be understood from the contributions of the phases detected, considering the relation $M_s = xM^{CuO} + xM^{Fe_2O_3} + (1-x)M^{CuFe_2O_4}$, where M_s is the experimental value observed at $H = 90$ kOe, and each superscript indicates the corresponding phase. The molar fraction x which leads to the observed value $M_s \approx 20$ emu g^{-1} is $x \approx 0.4$. This value does not contradict the relative amounts of haematite and spinel phases found from Mössbauer and x-ray data. However, since magnetization values may be somewhat lowered by the spin canting and ionic disorder effects detected in milled samples, the above estimation must be taken as a rough approximation only.

As mentioned in the results, the $M_R/M_s \approx 0.5$ values found for milled samples at 4.2 K suggest that the resulting particles are single domain with uniaxial anisotropy. For these particles the magnetic anisotropy energy is described by $E(\theta) = KV\sin^2\theta$, where K is the anisotropy constant, V the particle volume and θ the angle between the easy direction and the magnetization vector [19, 33]. The resulting superparamagnetic relaxation time τ depends on the KV product as

$$\tau = \tau_0 \exp[KV/kT] \tag{1}$$

where τ_0 is of the order of 10^{-10}–10^{-12} for ferro- and ferrimagnets [18, 33]. This dependence implies that a distribution of KV values will give relaxation times above and below the Mössbauer measuring time τ_m, leading to blocked and superparamagnetic particles respectively. Making use of previously reported values of anisotropy constants K of α-Fe_2O_3 and $CuFe_2O_4$ compounds [15, 22] and of equation (1), we estimated the ratio between both relaxation times of these phases. The obtained anisotropy energies led to $\tau(\alpha\text{-}Fe_2O_3)/\tau(CuFe_2O_4) \approx 1$, for given particle volume and temperature. Therefore, samples with similar particle sizes would display similar relaxation effects. This is observed in the Mössbauer spectra at 296 K of milled samples (figure 3) where the relaxation effects observed are nearly the same. However, a sextet can be observed for the CFM sample (see figure 3), revealing 23(4)% of particles with sizes well above the critical value. The same contribution of large α-Fe_2O_3 particles in sample CFM is observed at 4.2 K from the H1 signal, which amounts to 17(3)% of the total resonant area. No such contribution of large

particles is observed in the milled $CuFe_2O_4$ (CFS) sample. Since the obtained $\langle d \rangle$ values from x-ray data are coincident within error, the differences in Mössbauer spectra suggest different size distributions in milled CFM and CFS particles. The magnetic signal of the CFM sample implies that the distribution profile has a significant tail extending to the large-volume region (about $d > 20$ nm for the phases considered). The same considerations of anisotropy energies indicate that the absence of blocked particles in milled CFS may be originated in a narrower size distribution around the average $\langle d \rangle = 13$ nm value. This difference in the final particle distributions might be related to dissimilar hardnesses of the phases involved, which affect the grinding efficiency under the same experimental conditions [34, 35].

From the above discussion, the phase composition of milled samples can be explained assuming partial reversibility of the α-Fe_2O_3+CuO $\leftrightarrow$ $CuFe_2O_4$ reaction during milling. For the CFS sample, ball milling first reduces the particle size to the nanometre scale, which is followed by partial segregation of α-Fe_2O_3 and formation of $Cu_xFe_{3-x}O_4$ spinel. These two phases are composed of particles with sizes below the SPM critical size, at room temperature. For the CFM sample (CuO + α-Fe_2O_3 starting phases) the same initial reduction of particle size takes place, although a detectable amount of large haematite particles remains after 420 h of milling. Subsequently, formation of $Cu_xFe_{3-x}O_4$ phase takes place, presumably involving the smallest α-Fe_2O_3 particles produced. The proposed mechanisms are in agreement with a picture where mechanosynthesis consists of: (a) reduction of the grain size below a certain value and (b) the subsequent chemical reaction towards the equilibrium phase composition under the milling conditions.

In summary, we found that after 420 h of ball milling, different starting compositions of the Fe–Cu–O system evolved towards the same equilibrium composition of α-Fe_2O_3, CuO and spinel phases. Whereas the final $\langle d \rangle$ values were similar in both milled samples, the different particle size distributions yielded noticeable differences in magnetic behaviour. The resulting phase compositions were explained assuming partial reversibility of the CuO + α-Fe_2O_3 $\leftrightarrow$ $CuFe_2O_4$ reaction during milling. The spinel phase formed by milling was assigned to $Cu_xFe_{3-x}O_4$ ($0 < x < 1$) having cubic structure. The decrease of the grain size below a minimum value was found to be a necessary condition for chemical transformations between Fe–Cu–O phases to take place during milling.

Acknowledgments

Financial support from the Fundação de Amparo à Pesquisa do Estado de São Paulo is gratefully acknowledged.

References

[1] Ma E, He J H and Schilling P J 1997 *Phys. Rev.* B **55** 5542
[2] Tang Z X, Sorensen C M, Klabunde K J and Hadjipanayis G C 1991 *Phys. Rev. Lett.* **67** 3602
[3] Tejada J and Zhang X 1995 *J. Magn. Magn. Mater.* **140–144** 1815
[4] Thomas L, Lionti F, Ballow R, Gatteschi D, Sessoli R and Barbara B 1996 *Nature* **383** 145
[5] Morales M P, Serna C J, Bødker F and Mørup S 1997 *J. Phys.: Condens. Matter* **9** 5461
[6] Wernsdofer W, Orozco E B, Hasselbach K, Benoit A, Mailly D, Kubo O, Nakano H and Barbara B 1997 *Phys. Rev. Lett.* **79** 4014
[7] Zhang X, Hernandez J M, Tejada J and Ziolo R F 1996 *Phys. Rev.* B **54** 4101
[8] Richardson J T, Yiagas D I, Turk B, Forster K and Twigg M V 1991 *J. Appl. Phys.* **70** 6077
[9] See for example 1997 *7th Int. Conf. on Ferrites (Bordeaux) J. Physique Coll. IV* **7** C1
1998 *Proc. Int. Symp. Ferrites in Asia '97 (Tokyo, 1997)* at press
[10] Ding J, McCormick P G and Street R 1997 *J. Magn. Magn. Mater.* **171** 309
[11] Concas G, Congiu F and Bionducci M 1997 *J. Phys. Chem. Solids* **58** 1341

[12] See for example: Köster U 1997 *Mater. Sci. Forum* **235** 377
Battezzati L 1997 *Mater. Sci. Forum* **235** 317
Magini M and Iasonna A 1996 *Mater. Sci. Forum* **225** 229
Rustici M, Mulas G and Cocco G *Mater. Sci. Forum* **225** 243
Davis R M, McDermott B and Koch C C 1988 *Metall. Trans.* A **19** 2867
Weeber A W and Bakker H 1988 *Physica* B **153** 93
[13] Vanderberghe R E, Degrave E and De Bakker P M A 1994 *Hyperfine Interact.* **83** 29
[14] *Powder Diffraction Files of the Joint Committee on Powder Diffraction Data* (Swarthmore, PA: International Centre for Diffraction Data)
[15] Kündig W, Bömmel H, Constabaris G and Lindquist R H 1966 *Phys. Rev.* B **142** 327
[16] Goya G F 1997 *J. Mater. Sci. Lett.* **7** 563
[17] Evans B J and Hafner S 1968 *J. Phys. Chem. Solids* **29** 1573
[18] Tronc E and Jolivet J P 1997 *Mater. Sci. Forum* **235** 659
[19] Mørup S, Dumesic J A and Topsøe H 1980 *Applications of Mössbauer Spectroscopy* vol 2, ed R L Cohen (New York: Academic)
[20] Goya G F, Rechenberg H R and Jiang J Z 1998 *J. Appl. Phys.* **84** 1101
[21] Bhaduri M 1981 *J. Chem. Phys.* **75** 3674
[22] Krûpica S and Novak P 1982 *Ferromagnetic Materials* vol 3, ed E P Wolfarth (Amsterdam: North-Holland)
[23] Berkowitz A E and Schuele W J 1959 *J. Appl. Phys.* **30** 134S
[24] Xi S, Zhou J, Zhang D and Wang X 1997 *Mater. Lett.* **26** 245
[25] Schaffer G B and McCormick P G 1989 *App. Phys. Lett.* **55** 45
[26] Kaczmarek W A and Ninham B W 1997 *J. Physique Coll.* IV **7** C1 47
[27] Kosmac T and Courtney T H 1992 *J. Mater. Res.* **7** 1519
[28] Matteazzi P and Le Caër G 1991 *Mater. Sci. Eng.* A **149** 135
[29] Linderoth S, Jiang J Z and Mørup S 1997 *Mater. Sci. Forum* **235–238** 205
[30] Gerasimov K B, Gusev A A, Ivanov E Y and Boldyrev V V 1991 *J. Mater. Sci.* **26** 2495
[31] Morrish A H 1966 *The Physical Principles of Magnetism* (New York: Wiley)
[32] Smith J and Wijn H P J 1959 *Ferrites* (Philips' Technical Library)
[33] Mørup S 1990 *Hyperfine Interact.* **60** 959
[34] Forrester J S and Schaffer G B 1995 *Metall. Trans.* A **26** 725
[35] Schaffer G B and McCormick P G 1992 *Metall. Trans.* A **23** 1285